Check for updates

Received: 1 February 2024 | Revised: 5 March 2024 | Accepted: 6 March 2024

DOI: 10.1002/pen.26725

RESEARCH ARTICLE

POLYMER ENGINEERING AND SCIENCE WILEY

Aging properties of a vegetable-based polyurethane foam under high relative humidity and different temperatures

Enio Henrique Pires Da Silva[1] | **Silvio De Barros**[2,3] | **Pascal Casari**[4] | **Marcelo Leite Ribeiro**[1]

[1]Aeronautical Engineering Department, São Carlos School of Engineering, University of São Paulo, São Carlos, SP, Brazil

[2]CESI Lineact, Saint-Nazaire, France

[3]Federal Center of Technological Education (CEFET/RJ), Rio de Janeiro, RJ, Brazil

[4]CNRS, GeM, UMR 6183, Nantes Université, Ecole Centrale Nantes, Saint-Nazaire, France

Correspondence
Enio Henrique Pires Da Silva, Aeronautical Engineering Department, São Carlos School of Engineering, University of São Paulo, Av. João Dagnone 1100, São Carlos 13563-120, Brazil.
Email: eniopires@usp.br

Funding information
Conselho Nacional de Desenvolvimento Científico e Tecnológico, Grant/Award Number: 141012/2021-8; Coordenação de Aperfeiçoamento de Pessoal de Nível Superior, Grant/Award Number: 88887.716088/2022-00

Abstract

The objective of this study is to assess, characterize, and forecast the aging effects on the mechanical properties of a vegetable-based polyurethane foam (PUF) derived from castor oil under elevated relative humidity conditions and at two distinct load orientations (aligned with the expansion direction and perpendicular to it). Ten specimens were subjected to temperatures of 60, 75, and 90°C, along with a relative humidity of 90%, for a duration of up to 60 days. Compression tests, following ASTM D1621-16 standards and supplemented by 3D digital image correlation, revealed nearly isotropic behavior with marginally lower compression strength in the expansion direction. On the other hand, the strength of the foams at 90°C was higher in that direction. This led to a smaller activation energy (E_a) in this property, which ended up showing a shorter lifespan prediction considering the strength retention in this direction. The stiffness values were proportionally more similar in both directions than the strength ones and this was observed in the E_a for those curves. In contrast to several other foams and polyurethanes, the one examined in this study exhibited consistently higher E_a values for its mechanical properties, particularly in the transverse direction to expansion, surpassing 94 kJ/mol. This indicates a robust diffusion and chemical stability, suggesting its potential for prolonged utilization compared to conventional oil-based foams. A prediction was made that this foam would lose 50% of its stiffness and strength in around 9.8 and 9.5 years at 20°C, respectively, considering the directions more sensitive to the aging process. This research offers valuable insights for predicting lifespan based on operating temperatures and property retention needs, contributing to the advancement of sustainable materials in structural applications.

Highlights

- Fifty specimens investigated for each of two directions.
- Evaluation of vegetable-based PUF aging process unveils density changes.
- Unique behavior noted: different E_a values for each direction.
- High E_a values indicate enhanced mechanical stability over oil-based foams.
- Lifespan prediction enhances material application prospects.

 © 2024 Society of Plastics Engineers.

KEYWORDS
aging, activation energy, Arrhenius, compression, polyurethane

1 | INTRODUCTION

The search for new and eco-friendly raw materials for polymers has become the goal of numerous researchers as we have recognized the limitations and damages caused by oil extraction and refining.[1–3] Therefore, testing the properties of these eco-friendly polymers has been a major scientific subject in areas such as chemistry, physics, and engineering, with plenty of data available. However, the properties of these new materials after long-term exposure under different conditions are still an area with a scarce amount of data.

Polyurethane foam (PUF) is a significant polymeric cellular material utilized in a broad array of industrial applications, including automotive, furniture, aircraft, construction, and more.[4] The lifespan of PUFs varies depending on the type of exposure, ranging from 3 to more than 50 years. For instance, they typically have a lifespan of 15 years when used for refrigerator insulation. However, there is a dearth of scientific publications concerning the lifespan of PUFs, particularly where their mechanical properties are pertinent, such as in sandwich panels.[5] Furthermore, information regarding the durability and mechanical stability of vegetable-based PUFs over extended periods of time is even scarcer.

The development and characterization of bio-based PUs are demonstrating great potential as replacements for oil-based ones in the future, as many authors have focused their work on this subject.[6–8] Castor oil emerges as an economically viable and renewable resource, attracting significant research attention due to its applications in coatings, elastomers, sealants, and PUFs. Derived from the seeds of the *Ricinus communis* plant, a member of the Euphorbiaceae family, this oil is obtained through extraction or expression methods. Consequently, castor oil holds promise as a substitute for petroleum-derived polyol in the production of PUFs.[9] Lee et al.[10] developed bio-based PUFs using commercial castor oil as polyol and also experimented with castor oil combined with other additives. The authors studied the compression properties of these materials and reported compression strength (σ_c) values ranging from 250 to 550 kPa. Maiuolo et al.[11] synthesized PUFs from cellulose-based polyols and reinforced them with cellulose as well, manufacturing them with densities of 260 and 290 kg/m^3, respectively. The σ_c exhibited enhancement from 2.03 to 2.41 MPa, indicating successful application of cellulose reinforcement in a cellulose-based bio-polyol.

Overall, the mechanical properties of PUFs vary with their cellular structure, which is inherently linked to the manufacturing process.[12] The synthesis of most PUFs is based on the reaction between isocyanate, hydroxyl groups, and a blowing agent as follows: isocyanate reacts with hydroxyls, producing macromolecules built of urethane linkages that form the PU structure, while the reaction between isocyanate and a blowing agent generates gases (usually CO_2) that become trapped inside the PU structure, shaping the cells within the solid.[13,14] The size and distribution of cells within the foam directly impact its mechanical properties. Smaller and more uniform cells generally result in foams with higher strength and stiffness due to a greater amount of material surrounding each cell. The orientation of cells within the foam can impact its anisotropic mechanical properties. Foams with aligned or oriented cells exhibit directional strength properties, with higher strength along the direction of cell alignment and reduced strength perpendicular to it.[15,16]

The accelerated aging process in PUFs can be approached from various perspectives depending on the intended application and environmental exposure. UV aging is most relevant when the foam is to be used without protection from sunlight.[17] However, in many applications, PUFs are utilized indoors or with some form of superficial protection, rendering UV exposure negligible. Another aging approach involves considering the material's exposure to oxidative agents, with thermo-oxidation being the primary form of chemical degradation. The presence of oxygen does not directly influence the decomposition rate of PU into its raw materials but does affect the breakage of polymeric chains. Additionally, softer PU segments are more susceptible to oxidative degradation than harder ones, potentially leading to the appearance of scorching in degraded PUs.[18–20] Yarahmadi et al.[21] studied the aging of rigid PUFs in both air and nitrogen atmospheres. They reported that samples exposed to oxygen retained 88% of their initial weight after 60 days at 150°C, whereas those exposed to nitrogen retained 96% of their original weight under the same conditions. However, the authors observed no differences in flexural strength in this case. Gupta and Adhikari[22] investigated the thermo-oxidative degradation of PUs with varying chemical cross-link densities. They found that materials with higher cross-link densities exhibited greater retention of tensile strength after an aging period of 24 h at 100°C.

15482634, 0, Downloaded from https://4spepublications.onlinelibrary.wiley.com/doi/10.1002/pen.26725 by Univ of Sao Paulo - Brazil, Wiley Online Library on [19/04/2024]. See the Terms and Conditions (https://onlinelibrary.wiley.com/terms-and-conditions) on Wiley Online Library for rules of use; OA articles are governed by the applicable Creative Commons License

Hablot et al.[23] outlined some kinetic properties of the chemical reaction responsible for the synthesis of castor oil-polyurethanes. The authors utilized toluene diisocyanate (TDI), isophorone diisocyanate (IPDI), and hexamethylene diisocyanate (HDI) to synthesize PUs with castor oil as the polyol. They reported that the thermal stability was comparable for all diisocyanates. Concerning polymerization kinetics, the rate constant (k) order was found to be TDI > HDI > IPDI, and these values remained consistent for non-castor oil PUs.

Berardi[24] conducted a study where several PUFs were exposed for 4.5 months at 70°C. Additionally, the author investigated the conductivity of the materials under various relative humidity (RH) percentages. The author noted that closed-cell PUFs are less susceptible to conductivity changes when exposed to moisture and observed that the foam's conductivity increased over the duration of the study. By applying the Arrhenius equation to the thermal conductivity curves, the author estimated that exposure to 4.5 months at 70°C would correspond to degradation at room temperature over more than a decade.

In the presence of moisture, the mechanical properties of polymeric materials can undergo changes primarily due to three factors: water diffusion, erosion, and hydrolysis. Diffusion and erosion are linked to the physical structure of materials by disrupting hydrogen bonds when water penetrates between the chains (diffusion) or through mechanical removal of superficial layers of the material (erosion). While the former typically results in an increase in weight change, the latter typically leads to a decrease.[25,26] Concerning chemical degradation, hydrolysis often leads to the breakdown of molecular chains in aqueous environments, thereby compromising the integrity of materials, particularly under elevated temperatures, pH levels, or mechanical loads. These conditions have been shown to increase the likelihood of bond scission and, consequently, the hydrolysis rate in polymeric materials.[27–30] The influence of both phenomena can be predicted and described by determining the activation energy required to initiate such damage.[31] In the work of Hong et al.[32] the authors presented a methodology for predicting the lifespan of a PU elastomer using Arrhenius plots. They immersed their material in a solution of ethylene glycol and water for up to 32 days at temperatures ranging from 50 to 80°C. The authors observed an increasing weight change over time due to the absorption of the solution and a decreasing tensile strength resulting from the diffusion of the solution among the segments of the PU, which reduces the strength of the hydrogen bonds between the urethane segments. Additionally, through FT-IR spectroscopy, they found that in the presence of this solution, degradation via glycolysis reaction was stronger than hydrolysis. Finally, the authors used the Arrhenius equation to calculate the lifespan in accordance with the ASTM D2000 standard[33] and, based on the values of tensile strength, estimated a lifespan at room temperature of at least 10 years.

Therefore, the significance of understanding the degradation mechanisms exhibited by PUFs is unmistakably evident in numerous pivotal scientific studies, particularly when investigating vegetable-based PUFs. Thus, the primary objective of this study is to assess the alterations in the mechanical properties of a PUF derived from castor oil when exposed to elevated RH at varying temperatures. Furthermore, this research aims to contribute valuable insights into parameters necessary for predicting the aging behavior of this PUF under typical operational conditions at said RH level. By offering such predictive capabilities, this study serves as a vital resource for future endeavors seeking to leverage bio-based polymers effectively. It not only provides valuable data but also offers predictive tools, thereby facilitating advancements in the application of sustainable polymers in diverse fields. This approach not only enhances our understanding of bio-based PUFs but also lays the foundation for more informed decision-making and optimization of their performance in practical applications.

2 | MATERIALS

The PUF utilized in this study was procured from Kehl Company. It is a bi-component polymer, and the manufacturer provides the following information regarding the raw materials:

- Mineral-based methylene diphenyl diisocyanate (MDI) with a density of 1.22 g/cm^3 and viscosity ranging between 170 and 250 mPa·s at room temperature.
- Fully bio-based polyol derived from a blend of vegetable oils, primarily castor oil, with a density of 1.0 g/cm^3 and a viscosity of approximately 3000 mPa·s.

The PUF was synthesized in the GeM laboratory in Saint-Nazaire, France. Prior to the homogenization process, the raw materials were heated to 80°C in a convection oven. Subsequently, each component was poured into a plastic container in a 1:1 proportion, resulting in a total mass of 18 g. The reagents were then hand-homogenized for a few seconds until the expansion process commenced. Finally, the mixture was poured into a closed steel mold and allowed to cure for 30 min at 80°C until it was fully cured and ready to be stored away from light and moisture. This synthesis method is depicted in Figure 1.

15482634, 0, Downloaded from https://4spepublications.onlinelibrary.wiley.com/doi/10.1002/pen.26725 by Univ of Sao Paulo - Brazil, Wiley Online Library on [19/04/2024]. See the Terms and Conditions (https://onlinelibrary.wiley.com/terms-and-conditions) on Wiley Online Library for rules of use; OA articles are governed by the applicable Creative Commons License

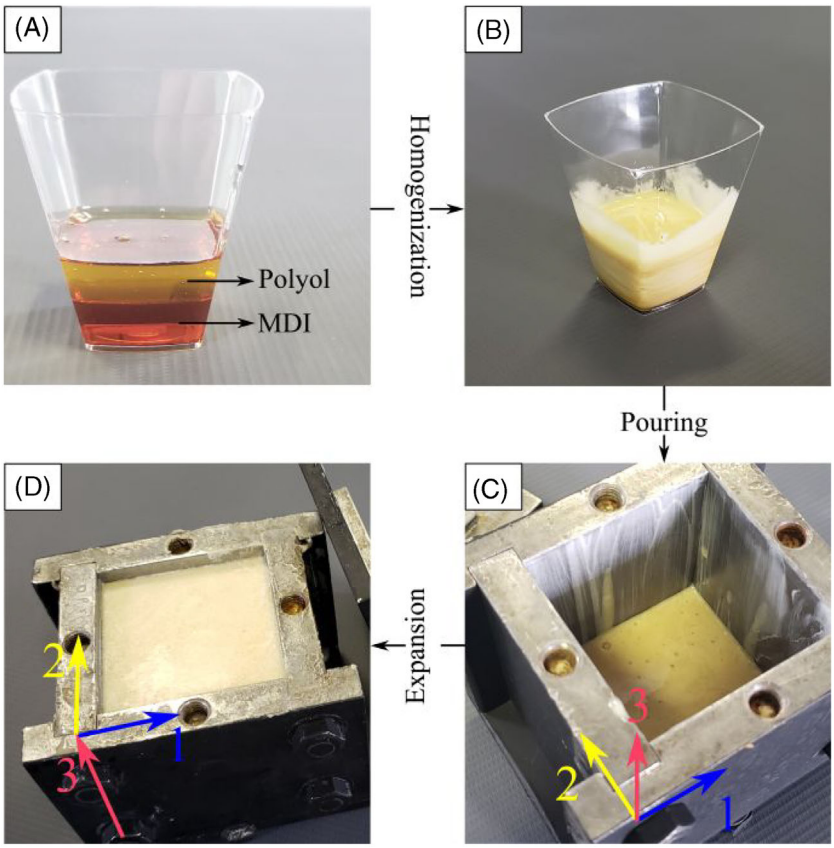

FIGURE 1 Phases of the synthesis process: (A) polyol and isocyanate in the plastic container, (B) mixture after homogenization, (C) mixture poured into the mold with indication of the expansion direction, and (D) PUF after curing.

3 | METHODS

Following the manufacture of the specimens, they were subjected to sanding using a dual-plate polishing machine by Presi to eliminate the layer effect caused by the closed-molding process. Subsequently, as the material was considered to be transversely isotropic, following the pattern commonly observed in cellular materials,[34,35] the labeling sequence was established as follows: direction 1 (Dir1) was aligned with direction 2 since both are transverse to direction 3 (Dir3), which represents the direction of expansion. These directions are illustrated in Figure 1C. Lastly, the dimensions of each direction were measured using a caliper, and the samples were weighed on a precision scale manufactured by Sartorius with a precision of 0.05 mg.

In order to investigate the microstructure of the foam and how it influences the material anisotropy, scanning electron microscope (SEM) images of the PUF were taken. The procedure was carried out using a Leo 440 Scanning Electron Microscope equipped with a secondary electron detector (SE1) and operated at an accelerating voltage of 15 kV. Prior to imaging, the samples were sputter-coated with a thin layer of conductive material (gold) using a BAL-TEC sputter coater to enhance their conductivity and minimize charging effects during imaging. The SEM images were captured at two different magnifications, 50 times for the foam structure before the tests with working distance (wd) of 45 and 47 mm, and 100 times for the foam after compression with wd of 32 and 30 mm.

3.1 | Aging process

The aging effect on material properties has been extensively documented to adhere to the Arrhenius equation governing the rates of chemical reactions, as depicted in Equation 1[36–38]:

$$K = A \exp \frac{-E_a}{RT}, \tag{1}$$

where K represents the Arrhenius degradation rate constant of the desired phenomenon; A is a pre-exponential and experimental factor; E_a denotes the activation energy for the respective phenomenon; R the universal gas constant (8.3145 J/K/mol); and T denotes the temperature in Kelvin (K). The Arrhenius relationship is founded on the premise that failure occurs due to chemical reactions or diffusion. As such, it assumes that after a critical amount of chemical reaction, the specimen will fail.

15482634, 0, Downloaded from https://4spepublications.onlinelibrary.wiley.com/doi/10.1002/pen.26725 by Univ of Sao Paulo - Brazil, Wiley Online Library on [19/04/2024]. See the Terms and Conditions (https://onlinelibrary.wiley.com/terms-and-conditions) on Wiley Online Library for rules of use; OA articles are governed by the applicable Creative Commons License

TABLE 1 Accelerated aging conditions for each batch of specimens.

Batch	Temperature (°C)	RH (%)	Time (days)
1	60	90	25
2	60	90	35
3	60	90	60
4	75	90	10
5	75	90	30
6	75	90	55
7	90	90	5
8	90	90	10
9	90	90	15

Consequently, this assumption implies that the time to failure (τ) is inversely proportional to K, as illustrated in Equation 2[39–41]:

$$\tau = A \exp \frac{E_a}{RT}. \tag{2}$$

During cataloging, the specimens were divided into batches of 10 specimens each (5 samples for Dir1 and 5 for Dir3). Three aging temperatures were selected to construct a comprehensive Arrhenius curve, based on previous studies conducted by various authors.[24,39,42] The maximum temperature of 90°C was selected for comparison with previous studies involving the same material.[43] The minimum temperature of 60°C was chosen to ensure the observation of a sufficient range of degradation for constructing an Arrhenius curve. Additionally, to prevent prolonged exposure of the material and maintain a substantial difference from the maximum temperature, 60°C was deemed ideal.

The high RH condition was applied in order to see how the foam would behave in comparison with a non-RH-controlled condition[43] where the effects of erosion, diffusion, and hydrolysis can take place along with the thermo-oxidation. To regulate the aging process, each batch was placed in a computer-controlled climate chamber (CC) manufactured by Climats. The specific accelerated conditions to which each batch was exposed are outlined in Table 1.

3.2 | Compression test methodology

The compression tests were conducted using a Zwick/Roell Z050 universal testing machine (UTM), with data directly acquired from its TestXpert II software at intervals of 0.1 s. The testing procedure adhered to the ASTM D1621-16 standard,[44] which has been widely utilized in numerous compression tests on foams in recent years.[45–47] In accordance with the standard, the test speed was set to 5 mm/min, and the specimen dimensions were approximately $50 \times 50 \times 50\ mm^3$ before the aging process. The test setup is illustrated in Figure 2. The strain values (ε) presented in this work are logarithmic strains calculated using Equation 3:

$$\varepsilon = \ln \frac{l}{l_0}, \tag{3}$$

where l represents the instantaneous length of the specimen and l_0 is its initial length. This strain calculation method was chosen due to the tests being conducted up to high deformations, indicating that the implementation of the subsequent compression data in numerical models would involve geometric nonlinearity.[48]

Five test specimens were utilized for each direction and aging condition, and the results are depicted as the mean values of each batch of 5, along with the standard deviation calculated using the *numpy.std* function from the numpy library in Python.

The longitudinal and transverse strains were determined using the 3D digital image correlation (DIC) technique. Images were captured by the VIC-3D system's dual-camera setup at intervals of 5 s. Prior to image capture, the system underwent calibration using eight calibration images to establish the distances between cameras and the specimen. The cameras were positioned with a 40 cm distance between lenses and a 53 cm distance between the lens and the specimen, creating a 45° angle between the specimen and the cameras. To measure strain values in both directions, two virtual extensometers were positioned in the middle of the specimens, one vertically and one horizontally.

The general compression behavior of foams can be classified into three main categories: elasticity of the cell walls; plastic deformation of the cell walls under constant load (plateau); and densification hardening after the full collapse of the cells. The flat or plateau region is particularly important as it largely comprises pure plastic deformation, contributing significantly to the foams' exceptional energy absorption capacity. The specific energy, defined as the work per unit volume, represents the area beneath the stress–strain graph and can be calculated using Equation 4[49]:

$$U = \int_0^{\varepsilon} \sigma(\varepsilon) d\varepsilon. \tag{4}$$

Furthermore, the efficiency of energy absorption can be described as the ratio between the specific energy and

15482634, 0, Downloaded from https://4spepublications.onlinelibrary.wiley.com/doi/10.1002/pen.26725 by Univ of Sao Paulo - Brazil, Wiley Online Library on [19/04/2024]. See the Terms and Conditions (https://onlinelibrary.wiley.com/terms-and-conditions) on Wiley Online Library for rules of use; OA articles are governed by the applicable Creative Commons License

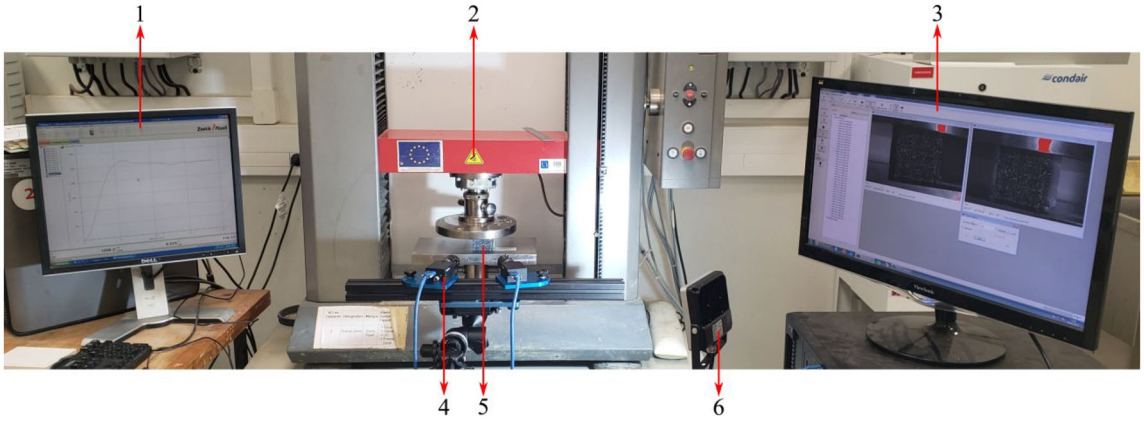

FIGURE 2 Test scheme where 1 is the computer controlling the UTM, 2 is the crosshead of the UTM, 3 is the computer controlling the DIC Vic-Snap software, 4 is one of the two cameras for the 3D DIC, 5 is the test specimen, and 6 is the lightning device.

stress. This measure offers a more suitable representation of a material's ability to absorb energy, as it takes into account the applied stress level. The energy absorption efficiency can be calculated using Equation 5:

$$\eta = \frac{\int_0^{\varepsilon} \sigma(\varepsilon) d\varepsilon}{\sigma(\varepsilon)}, \tag{5}$$

where U is the deformation energy, η is the energy absorption efficiency, and $\sigma(\varepsilon)$ is the stress at its respective strain level.[50]

3.3 | Degradation curves methodology

The mass and volume changes are calculated as percentages, determined by the ratio between the average properties before and after exposure to the CC. The density variation after the aging processes is reported using a probability density function, as illustrated in Equation 6, calculated by the *scipy.stats.norm* tool in Python:

$$f(x) = \frac{\exp\left(-\frac{x^2}{2}\right)}{\sqrt{2\pi}}, \tag{6}$$

where $f(x)$ is the probability density function and x is a real number (density of each cube in this case).

The calculation of property retention (%) is essential for determining Arrhenius parameters, such as E_a, through the construction of an Arrhenius plot.[51] Consequently, this study provides values for elasticity modulus retention (E_r) and compression strength retention (S_r) following each accelerated aging condition. As illustrated in Figure 3, it becomes feasible to compute the properties required for the application of the Arrhenius equation (Equation 1), including E_a.

As depicted in Figure 3A, selecting a property retention value (P_r) necessitates identifying its corresponding incubation time in the CC (t) for each temperature (T). To properly linearize the parameters, at least three temperature values are required. Subsequently, by plotting the log of the reaction rate (the inverse of t) on the vertical axis and the reciprocal of T on the horizontal axis, E_a can be calculated from the slope of the curve depicted in Figure 3B, where T_r and t_r represent the actual or operational temperature and time under non-accelerated conditions corresponding to the chosen P_r.

Consequently, it becomes feasible to predict the t_r required until a specified value of P_r has been attained, thereby defining the material's lifespan.

4 | RESULTS

The mass change over time of the PUF is depicted in Figure 4A. Initially, there was an increase in mass across all temperatures, which is expected due to water diffusion into the polymer. However, a notable difference in mass increase is evident at 90°C. This variation can be attributed to the Arrhenius model, where temperature variation exponentially modifies the reaction rate. In this case, as water contributes to the thermo-oxidation reaction, significant mass loss was observed at 90°C. Following the initial mass gain, a logarithmic mass loss pattern was observed. For the 60°C specimens, the mass loss was insufficient to exceed the mass gain from water diffusion, resulting in specimens even after 60 days in the CC retaining a higher mass than their initial one. At 75°C, average mass loss values of 0.31% and 0.35% were observed after 30 and 55 days in the CC, respectively, indicating that at this

15482634, 0, Downloaded from https://4spepublications.onlinelibrary.wiley.com/doi/10.1002/pen.26725 by Univ of Sao Paulo - Brazil, Wiley Online Library on [19/04/2024]. See the Terms and Conditions (https://onlinelibrary.wiley.com/terms-and-conditions) on Wiley Online Library for rules of use; OA articles are governed by the applicable Creative Commons License

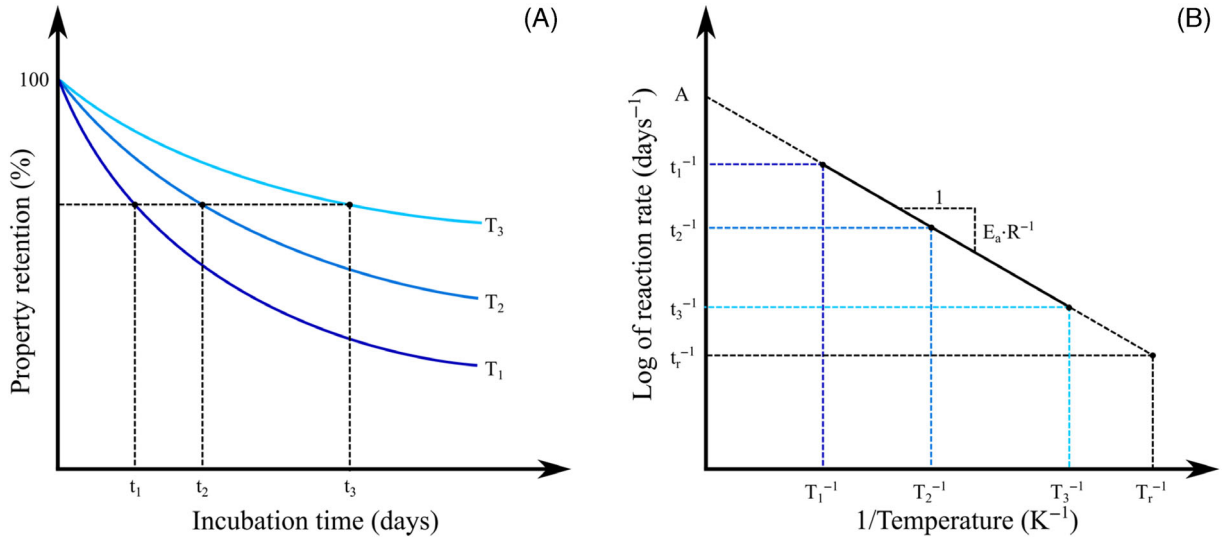

FIGURE 3 (A) Property retention plot over time in the acceleration condition, (B) Arrhenius plotting scheme (developed from[25]).

temperature, the mass loss should not exhibit considerable variation over time, as it appears to be approaching an asymptotic point. Finally, specimens exposed to 90°C in the CC exhibited significant mass loss, reaching 1.02% after 15 days, with no indication of nearing an asymptotic value.

The thermo-oxidative degradation in an elevated humidity degradation plays a critical role in dictating the degradation kinetics and mechanisms of this material. Elevated RH environments introduce additional complexities compared to drier conditions. At higher humidity levels, the presence of water molecules facilitates the penetration of oxygen into the foam matrix, accelerating oxidation reactions, this can be interpreted by the increasing mass in the first days of elevated humidity exposure. This heightened oxygen availability promotes more extensive chain scission, leading to increased fragmentation and degradation of the polymer backbone. Additionally, water molecules can directly participate in hydrolytic degradation processes, further weakening the polymer network. Conversely, in drier environments, the reduced presence of water restricts both oxygen diffusion and hydrolysis, resulting in a comparatively slower degradation rate characterized by primarily thermo-oxidative mechanisms.

The dimensional changes depicted in Figure 4B show variations in length in the three directions relative to their respective initial values. After 60 days at 60°C, the specimens exhibited slight enlargement, particularly in Dir3, noticeable as a small bump appearing in the center of each direction. A similar, albeit much smaller bump was observed in specimens exposed to 75°C in the CC. Yarahmadi et al.[21] demonstrated that while the cross-sectional area changes in an environment with air, it remains unchanged in an environment with pure nitrogen at the same temperature of 150°C. The authors reported nearly a 25% increase in cross-sectional area after 30 days, attributing this behavior to thermo-oxidation. However, specimens heated at 90°C showed substantial shrinkage values, up to 13.6% after 15 days of exposure. This characteristic was attributed to gas leakage from the cells, resulting from elevated pressure due to high temperature (which explains the previous foams' enlargement), alongside weakening of the polymeric structure also due to temperature, potentially causing the leakage that shrank the specimens. Consequently, density variation after accelerated aging was predominantly evident in specimens exposed to 90°C. Al-Moameri et al.[52] suggested that to decrease the shrinkage of a vegetable-based PUF, elevated reagent and curing temperatures are advisable, as the number of cross-linked chains increases with temperature, leading to a stiffer polymeric structure of the cell walls. Thus, the assumption that the shrinkage observed in the present study resulted from decreased stiffness of the cell walls due to elevated temperature, rather than manufacturing flaws, appears reasonable.

The average density for the pristine foams is 85.20 kg/m^3, considering the mass and dimensions measured before the aging process for all nine batches. First, Figure 5 illustrates the normal distribution for the samples separated by the temperature to which they were exposed. As the dimensional and mass changes were minimal for the specimens subjected to 60°C, their density remained unchanged after the aging process. Second, for the specimens aged at 75°C, dimensional shrinkage after 55 days increased the average density to 91.93 kg/m^3, while density numbers for shorter periods

15482634, 0, Downloaded from https://4spepublications.onlinelibrary.wiley.com/doi/10.1002/pen.26725 by Univ of Sao Paulo - Brazil, Wiley Online Library on [19/04/2024]. See the Terms and Conditions (https://onlinelibrary.wiley.com/terms-and-conditions) on Wiley Online Library for rules of use; OA articles are governed by the applicable Creative Commons License

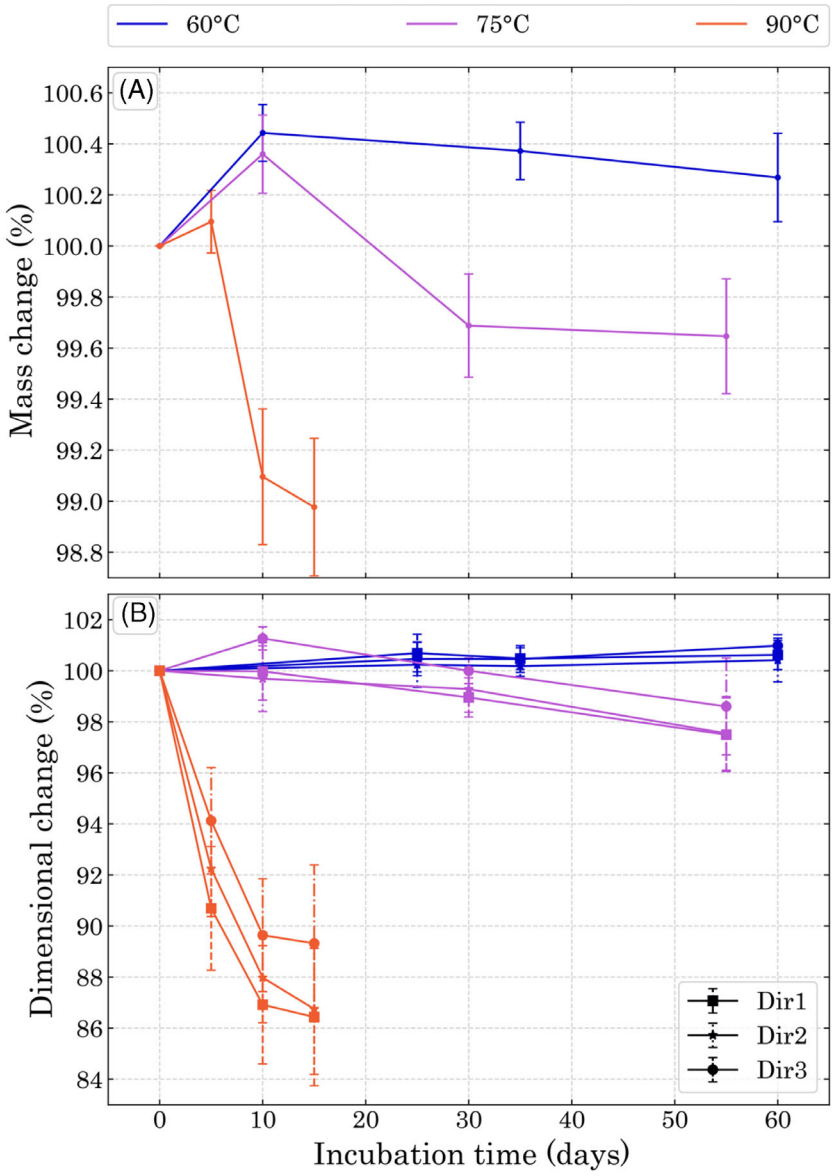

FIGURE 4 (A) Mass change and (B) dimensional change.

of time were close to the pristine value. Finally, the density observed after all incubation periods at 90°C exhibited an increasing average, as the shrinkage phenomenon was prominent after 5 days of exposure, reaching an average of 133.34 kg/m^3 after 15 days. Table 2 summarizes the average values depicted in Figures 4 and 5, along with their respective standard deviation values.

4.1 | Anisotropy analysis

Our study delves into the intricate relationship between cellular morphology and mechanical characteristics of this bio-based foam. Figure 6 shows its SEM images for planes (A) 3—1 and (B) 2—1. Figure 6 (C) and (D) are the tested samples for the respective planes. Notably, we observed a distinctive pattern in cell shape orientation: cells aligned along the expansion direction exhibited elongated hexagonal shapes, while those perpendicular to it tended towards elliptical forms, approaching circularity. This asymmetrical arrangement impacted the mechanical response of the foam, with cells oriented in the hexagonal direction demonstrating notably lower yield strength compared to their counterparts in the elliptical orientation. This might be attributed to a long-beam-like shape of the elongated hexagon, which may add buckling as a major failure mechanism to its cell walls. This can be observed by a much higher number of cell walls damaged in the middle of its longitudinal span as seen in Figure 6C than the cell walls in Figure 6D.

Figure 7A,B shows the compression test results for all the nine batches for Dir1 and Dir3, respectively. The differences between Dir3 and Dir1 in the elastic zone lie in the yield strength, where σ_c was 351 ± 30 and 402 ± 46, respectively.

15482634, 0, Downloaded from https://4spepublications.onlinelibrary.wiley.com/doi/10.1002/pen.26725 by Univ of Sao Paulo - Brazil, Wiley Online Library on [19/04/2024]. See the Terms and Conditions (https://onlinelibrary.wiley.com/terms-and-conditions) on Wiley Online Library for rules of use; OA articles are governed by the applicable Creative Commons License

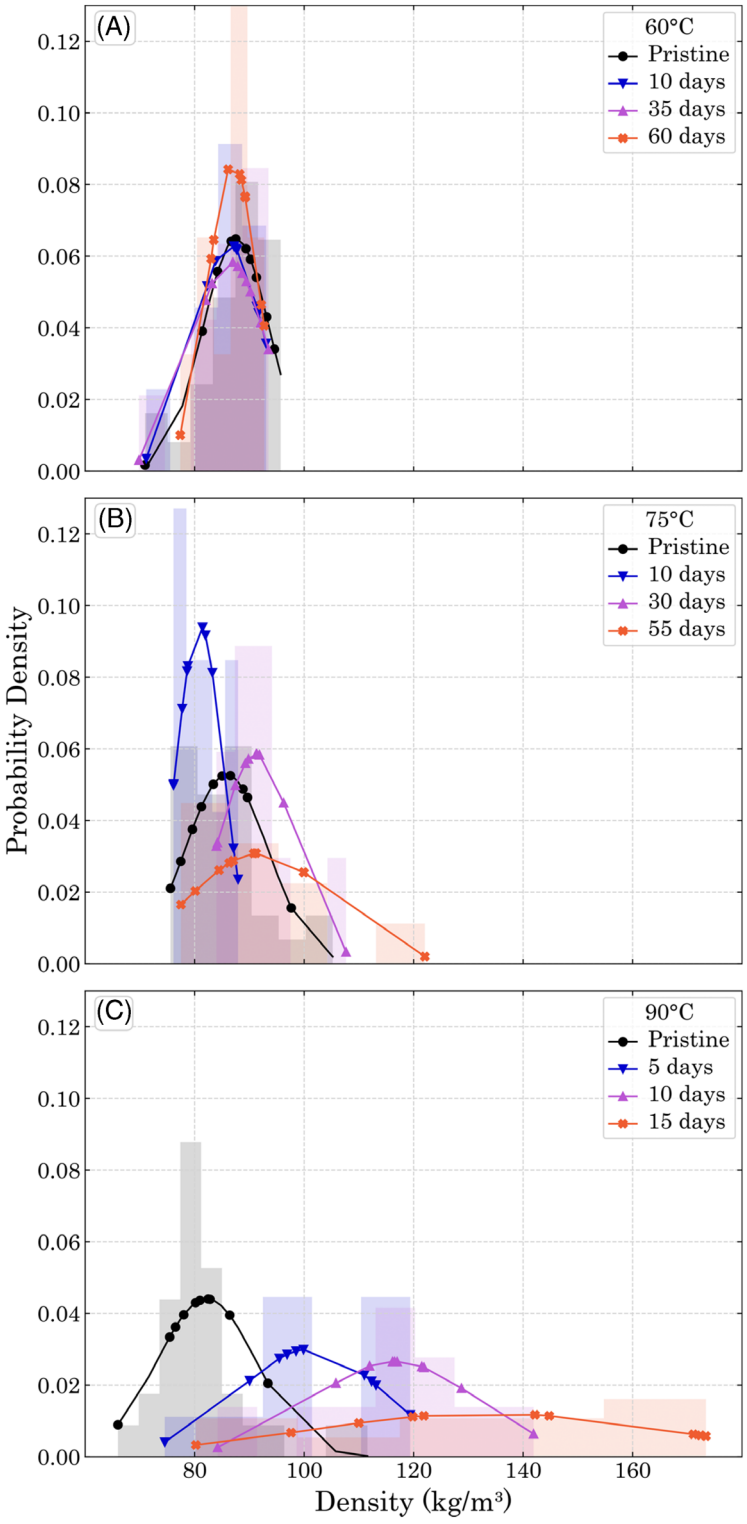

FIGURE 5 Density variation probability function.

This directional dependence can be exploited in applications where tailored mechanical properties are required, such as in structural supports or impact absorption systems. For example, in composite materials where PUF serves as a core or filler, its anisotropic nature can influence the overall mechanical stability of the material, since Dir1 can handle a higher amount of load, it would present a higher flexure strength than Dir3 because core materials tend to fail due to compression or shear in sandwich structures.

The anisotropic behavior is not significantly pronounced in the plateau region, and considering the deviation displayed by each batch, the materials can be considered almost isotropic within this interval. However, at higher strains, the discrepancies between Dir1 and Dir3

15482634, 0, Downloaded from https://4spepublications.onlinelibrary.wiley.com/doi/10.1002/pen.26725 by Univ of Sao Paulo - Brazil, Wiley Online Library on [19/04/2024]. See the Terms and Conditions (https://onlinelibrary.wiley.com/terms-and-conditions) on Wiley Online Library for rules of use; OA articles are governed by the applicable Creative Commons License

TABLE 2 Physical properties variation among the batches.

Batch	Mass retention (%)	Length change (%)			Average density (kg/m^3)
		Dir1	Dir2	Dir3	
Pristine	–	–	–	–	85.20 ± 7.88
1	100.44 ± 0.17	100.69 ± 0.74	100.24 ± 0.89	100.46 ± 0.65	86.30 ± 5.97
2	100.37 ± 0.17	100.48 ± 0.42	100.18 ± 0.39	100.46 ± 0.52	86.37 ± 6.46
3	100.27 ± 0.26	100.62 ± 0.57	100.42 ± 0.86	100.98 ± 0.43	87.01 ± 4.41
4	100.36 ± 0.23	99.98 ± 1.13	99.69 ± 1.29	101.28 ± 0.45	80.91 ± 4.00
5	99.69 ± 0.30	98.96 ± 0.76	99.28 ± 0.90	100.00 ± 0.50	91.30 ± 6.47
6	99.65 ± 0.34	97.49 ± 1.44	97.55 ± 1.44	98.60 ± 1.90	91.93 ± 12.23
7	100.10 ± 0.18	90.69 ± 2.42	92.25 ± 2.50	94.13 ± 2.78	101.11 ± 12.60
8	99.10 ± 0.40	86.92 ± 3.32	87.98 ± 4.34	89.64 ± 4.95	116.56 ± 14.24
9	98.98 ± 0.40	86.43 ± 6.69	86.75 ± 5.42	89.32 ± 7.10	133.34 ± 31.18

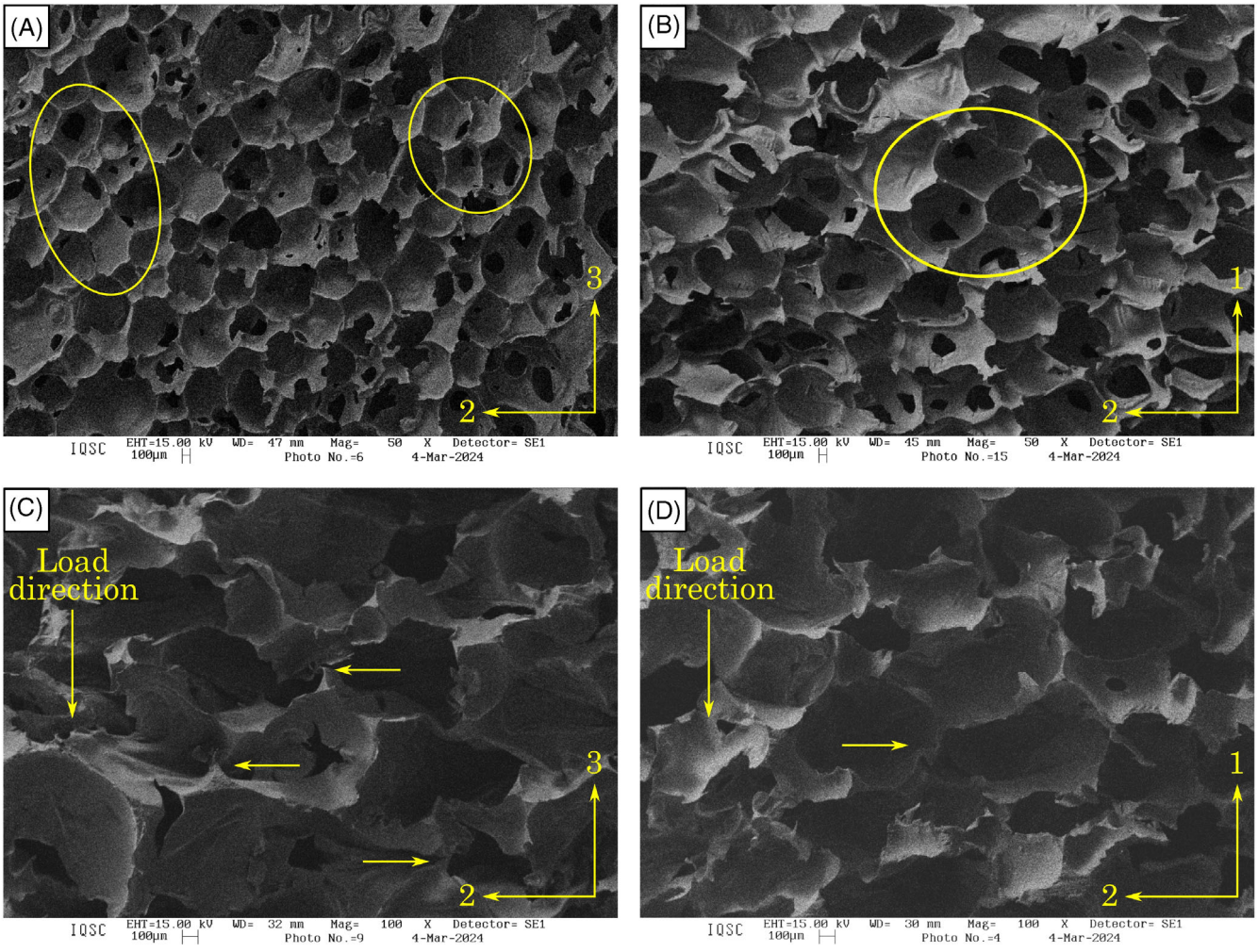

FIGURE 6 SEM images of the foam structure in planes (A) 2-3 and (B) 2-1 and crushed samples in the respective planes for (C) and (D).

become more pronounced. This behavior will primarily impact applications related to plastic energy absorption. Therefore, Figure 8 illustrates the η-strain curves for each batch in (A) Dir1 and (B) Dir3.

The maximum energy absorption efficiency (η_{max}) was higher for specimens in Dir1 than those tested in Dir3. This trend is also evident in the strain limits depicted in Figure 7, where the values for Dir3 are

15482634, 0, Downloaded from https://4spepublications.onlinelibrary.wiley.com/doi/10.1002/pen.26725 by Univ of Sao Paulo - Brazil, Wiley Online Library on [19/04/2024]. See the Terms and Conditions (https://onlinelibrary.wiley.com/terms-and-conditions) on Wiley Online Library for rules of use; OA articles are governed by the applicable Creative Commons License

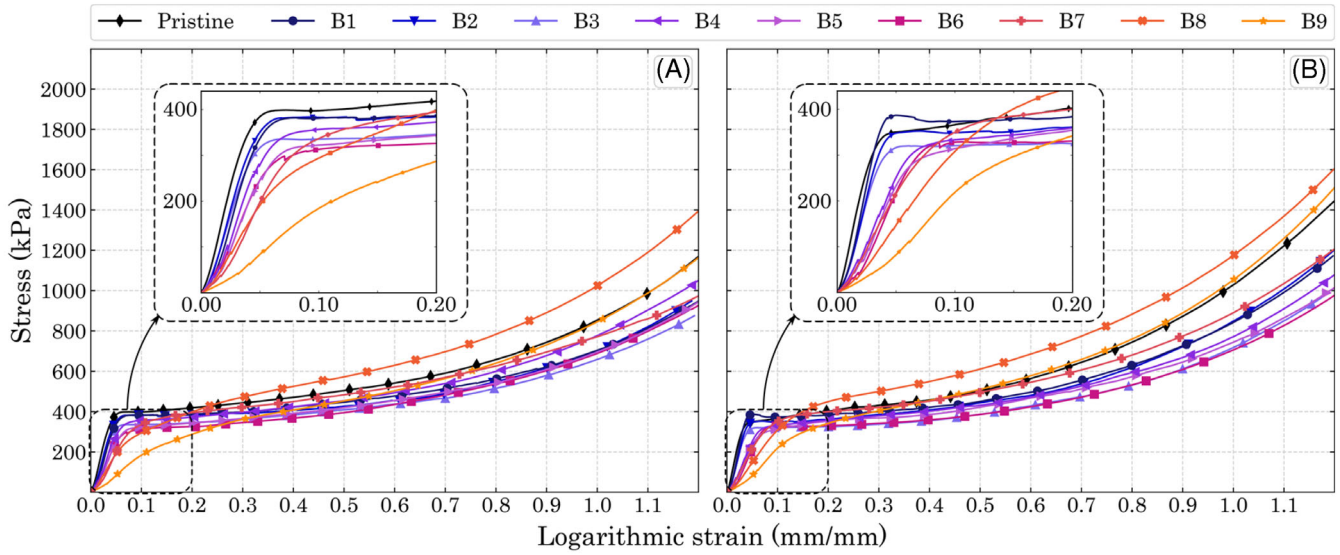

FIGURE 7 Compression test results for all batches in (A) Dir1 and (B) Dir3.

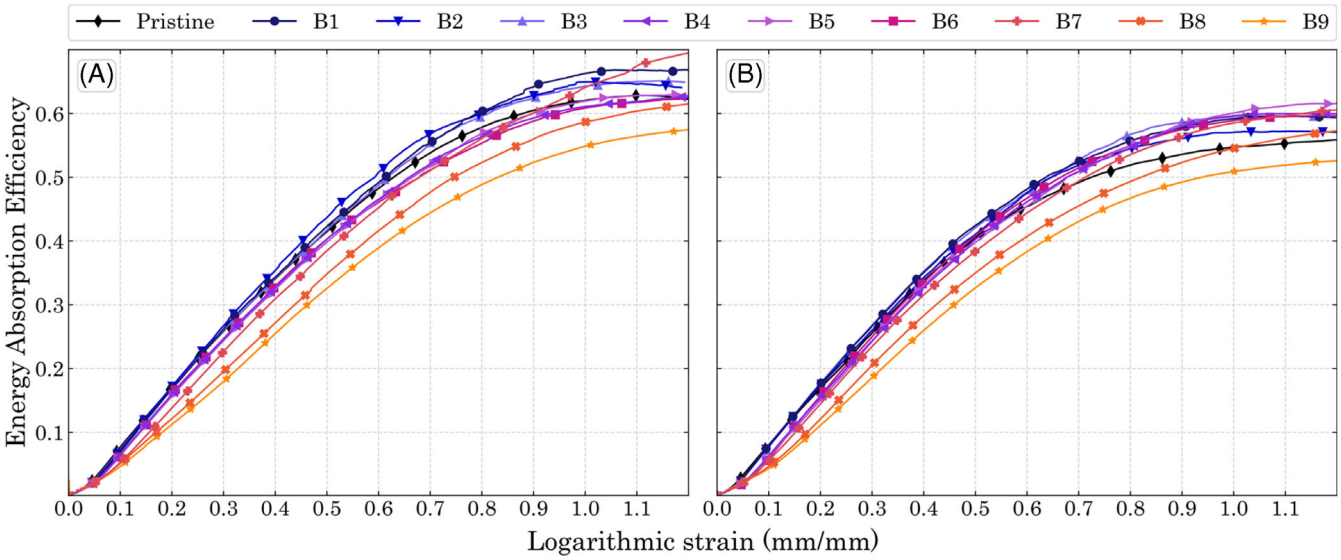

FIGURE 8 Energy absorption efficiency for all batches in (A) Dir1 and (B) Dir3.

approximately 200 kPa higher than those for Dir1. This suggests that Dir1 can absorb more plastic energy than Dir3 under the same load at higher strains. However, despite exhibiting different plastic behaviors at elevated displacements, the strain values at which the maximum energy absorption efficiency occurs ($\varepsilon_{\eta max}$) were similar between Dir1 and Dir3. This indicates that densification (the drop in energy absorption efficiency) occurs at the same displacement for both directions. Table 3 summarizes the values presented in Figures 7 and 8 for Dir1 and Dir3.

The DIC analysis successfully provided data for some of the batches, while for others, due to misalignment and/or excessively large dimensional changes, the DIC analysis did not yield reliable data. Additionally, during the tests, the speckle pattern painted over the samples tore, particularly under strain values exceeding 10%. Moreover, variations were observed at the beginning of the tests due to sample accommodation. Therefore, Figure 9 illustrates Poisson's ratio (ν) for logarithmic strain values ranging from 2% to 6.5%, representing most of the elastic area. In this interval, we have observed a homogeneous initial behavior in the middle of the samples. In the plastic regime, there is a considerable amount of strain accumulation in specific and random areas of the specimens, this is why our Poisson's ratio analyses go up to 6.5% of strain. Therefore, the analyses of the Poisson's ratio are reliable within this regime since both

15482634, 0, Downloaded from https://4spepublications.onlinelibrary.wiley.com/doi/10.1002/pen.26725 by Univ of Sao Paulo - Brazil, Wiley Online Library on [19/04/2024]. See the Terms and Conditions (https://onlinelibrary.wiley.com/terms-and-conditions) on Wiley Online Library for rules of use; OA articles are governed by the applicable Creative Commons License

TABLE 3 Compression properties variation among the batches.

		Pristine	1	2	3	4	5	6	7	8	9
σ_c kPa	Dir1	402 ± 46	382 ± 53	383 ± 21	335 ± 67	355 ± 51	320 ± 65	314 ± 56	330 ± 54	260 ± 53	200 ± 62
	Dir3	351 ± 30	386 ± 40	349 ± 41	305 ± 42	331 ± 32	294 ± 39	327 ± 31	340 ± 60	360 ± 40	270 ± 55
E kPa	Dir1	10,907 ±935	9076 ±797	8565 ±546	7515 ±1261	7190 ±1109	5619 ±875	4515 ±701	4781 ±740	2951 ±992	1525 ±445
	Dir3	11,034 ±1152	8573 ±1038	7662 ±1234	6357 ±907	5883 ±658	5713 ±802	4984 ±631	5279 ±443	2891 ±398	2103 ±326
η_{max} %	Dir1	62.8 ±1.5	67.0 ±4.7	65.0 ±3.6	65.1 ±1.1	62.6 ±2.2	63.0 ±5.3	62.5 ±4.8	73.9 ±14.7	66.3 ±17.1	61.7 ±13.1
	Dir3	56.3 ±1.0	59.6 ±4.0	57.2 ±2.8	59.6 ±3.5	60.0 ±3.5	61.6 ±4.2	59.6 ±1.5	61.6 ±9.0	61.0 ±7.3	55.6 ±8.8
$\varepsilon_{\eta max}$	Dir1	1.119 ±0.021	1.201 ±0.010	1.018 ±0.009	1.141 ±0.015	1.190 ±0.033	1.174 ±0.026	1.204 ±0.048	1.551 ±0.103	1.633 ±0.221	1.666 ±0.278
	Dir3	1.275 ±0.017	1.103 ±0.018	1.130 ±0.011	1.114 ±0.005	1.168 ±0.031	1.200 ±0.019	1.171 ±0.037	1.388 ±0.138	1.623 ±0.088	1.640 ±0.268

transverse and longitudinal extensometers were positioned in the center of the specimens.

There was no notable difference among the batches for Dir1 within the considered valid strain range. The ν ranged from around 0.35 to 0.2. It's noteworthy that the Poisson's ratio showed a tendency to decrease with increasing strain. Additionally, as the foam cells collapse in the plastic zone, it can be affirmed that volume is not conserved during plasticity. The areas that experienced strain concentration, as highlighted in Figure 10, shrink and collapse until densification begins. Meanwhile, the ν remains close to 0 in the rest of the specimen until a new area of concentrated strain begins to collapse, and the speckle pattern in the previous concentration area becomes unrecognizable, as shown in Figure 10.

The ν for Dir3 exhibited higher deviation compared to Dir1, and the decrease with increasing strain was more pronounced. Once again, no clear pattern was identified for Dir3. However, in this direction, the VIC-3D software managed to recognize speckle deformation for a few specimens in batch number 7 (the only one in Figure 9 exposed to 90°C), and the ν was approximately 50% smaller than most of the other batches. This may suggest that the shrinkage caused by the 90°C exposure could decrease the Poisson's ratio of the material. However, due to the significant deviation among the specimens, drawing further conclusions becomes challenging.

4.2 | Degradation curves

Using the data provided in Table 3, it was possible to estimate the Sr and Er for each batch. Subsequently, P_r values of 95%, 90%, and 85% were selected, as all the batches exhibited retention values within this range, with the smallest P_r (approximately 85%) being σ_c for Dir3 at 60°C. Therefore, it was not feasible to calculate E_a for less than 85% of P_r, since only two temperatures achieved this value for all properties. Finally, through interpolation, the time ($t1$, $t2$, and $t3$) taken at each temperature ($T1 = 90°C$, $T2 = 75°C$, and $T3 = 60°C$) to reach the chosen P_r was determined. This procedure was guided by Figure 3A, and the obtained times are presented in Table 4.

The times increased as the temperatures decreased ($t3 > t2 > t1$) for all P_r values except for the S_r95%, where $t1$ was 11.5 days and $t2$ was 8.79 days, which contradicts what is expected according to Equation 1, since this was a singular exception and the standard deviation in the compression strength values showed numbers around 10%, this anomaly can be attributed to variations in mechanical test results due to the porous characteristic of the material. For all the acquired times regarding S_r, the

15482634, 0, Downloaded from https://4spepublications.onlinelibrary.wiley.com/doi/10.1002/pen.26725 by Univ of Sao Paulo - Brazil, Wiley Online Library on [19/04/2024]. See the Terms and Conditions (https://onlinelibrary.wiley.com/terms-and-conditions) on Wiley Online Library for rules of use; OA articles are governed by the applicable Creative Commons License

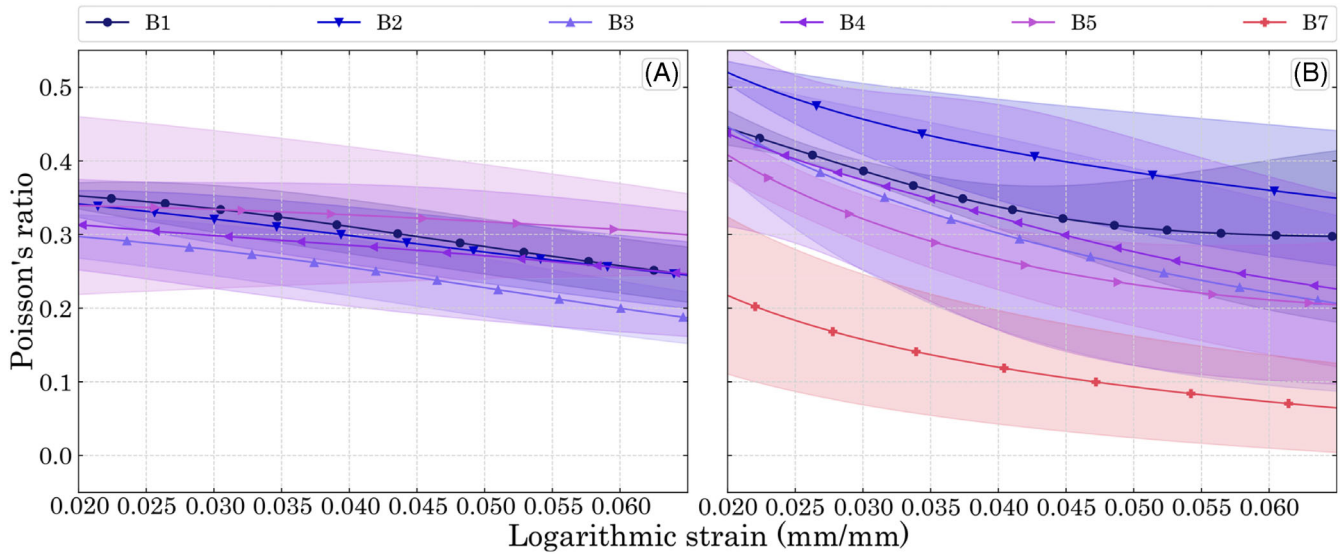

FIGURE 9 Poisson's ratio for (A) Dir1 and (B) Dir3.

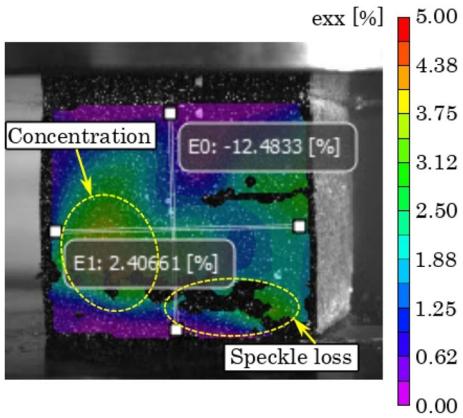

FIGURE 10 Strain concentration in the center of the specimen.

TABLE 4 Time until reaching the chosen P_r for each temperature.

P_r		t_1 (days)	t_2 (days)	t_3 (days)
$S_r = 95\%$	Dir1	1.41	4.44	36.5
	Dir3	11.5	8.79	43.8
$S_r = 90\%$	Dir1	2.88	8.89	46.9
	Dir3	12.5	18.1	53.7
$S_r = 85\%$	Dir1	4.23	18.5	57.5
	Dir3	13.4	27.6	60
$E_r = 95\%$	Dir1	0.45	1.52	7.32
	Dir3	0.45	1.11	5.56
$E_r = 90\%$	Dir1	0.91	2.93	14.9
	Dir3	0.96	2.12	11.1
$E_r = 85\%$	Dir1	1.31	4.44	22.2
	Dir3	1.41	3.23	16.9

Dir3 numbers were higher than their respective Dir1 times. Conversely, in E_r times, all the respective times of Dir1 were higher than Dir3, except for $t1$ at 95% E_r when they were the same. Although this behavior could also be due to deviation among the samples or some sort of material heterogeneity, another possibility is that this pattern could be related to the accelerated aging process, where the samples were placed inside the chamber and left there to age in the same position over a stainless-steel grill, and the conductivity of the grill could have influenced the bottom side of the specimens differently than the other sides.

Figures 11 and 12 show the Arrhenius plots for S_r and E_r, respectively, at times $t1$, $t2$, and $t3$, temperatures of 363.15 K, 348.15 K, and 333.15 K, and retention levels of 95%, 90%, and 85%. Most of the points were almost perfectly linearized, particularly those in Dir1, where five out of six coefficients of determination (R^2) were 0.99. The linearized plots in Dir3 deviated more from their scatter points, with R^2 values ranging from 0.61 to 0.99. This discrepancy can be explained by the behavior of S_r95%, which did not adhere to the Arrhenius law. Excluding this value, the other curves in Dir3 were reasonably well-fitted, especially for E_r, where R^2 ranged from 0.96 to 0.97.

The E_a/R values for strength and stiffness are not necessarily the same, as observed in Figures 11 and 12. This discrepancy can occur because the degradation mechanisms may differ for strength and stiffness. In stiffness, they might be primarily influenced by the breaking of chemical bonds within the polymer chains, which could

15482634, 0, Downloaded from https://4spepublications.onlinelibrary.wiley.com/doi/10.1002/pen.26725 by Univ of Sao Paulo - Brazil, Wiley Online Library on [19/04/2024]. See the Terms and Conditions (https://onlinelibrary.wiley.com/terms-and-conditions) on Wiley Online Library for rules of use; OA articles are governed by the applicable Creative Commons License

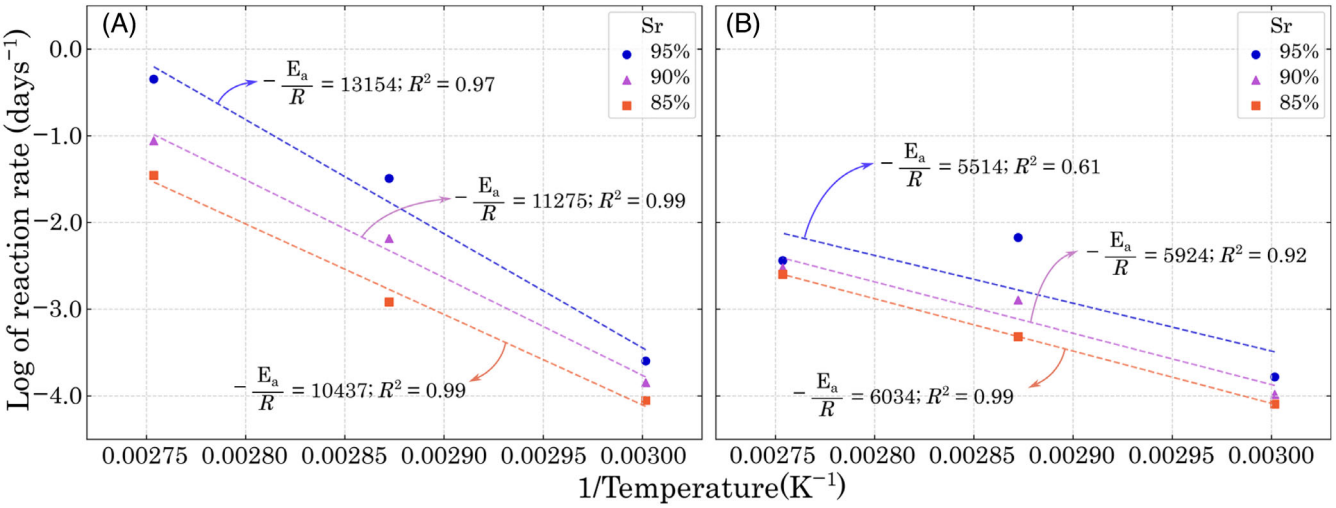

FIGURE 11 Arrhenius plot for strength retention in (A) Dir1 and (B) Dir3.

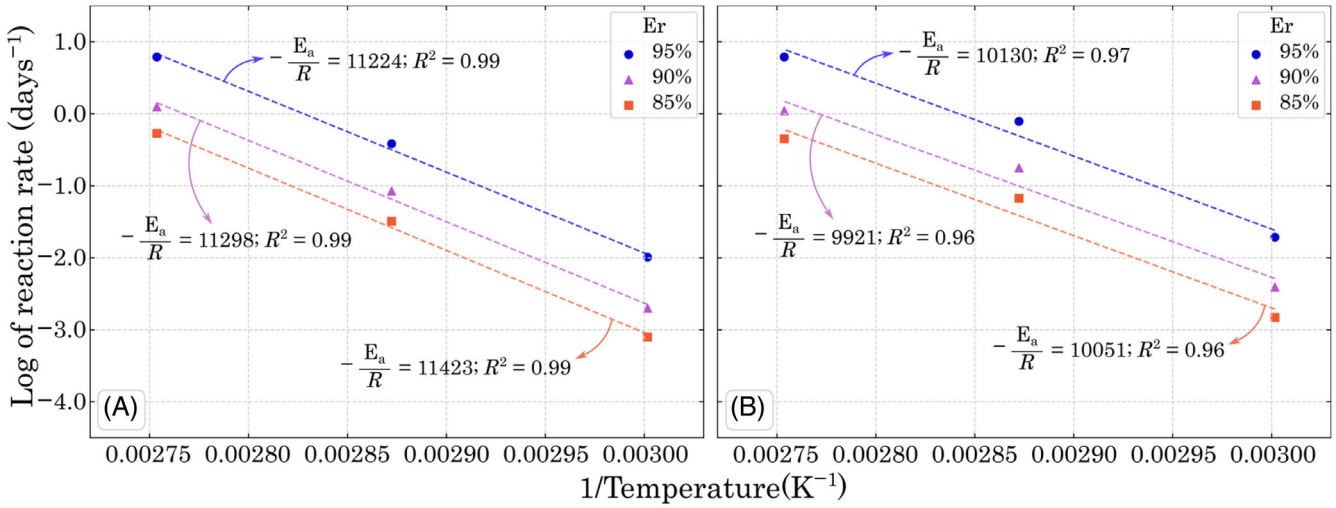

FIGURE 12 Arrhenius plot for stiffness retention in (A) Dir1 and (B) Dir3.

have one activation energy associated with it. On the other hand, degradation in strength might be more related to the formation and propagation of defects within the material, which could involve a different set of activation energies.[53]

The activation energies of degradation in stiffness ($E_a{}^E$) were 94.08 ± 0.84 kJ/mol and 83.43 ± 0.88 kJ/mol for Dir1 and Dir3, respectively. This implies that more energy is necessary to interfere with the stiffness properties in Dir1 than in Dir3. It is noteworthy how close the $E_a{}^E$ values are between both directions, suggesting an isotropic activation energy for stiffness. However, the activation energy values for degradation in compression strength ($E_a{}^\sigma$) were higher in Dir1 than in Dir3, ranging from 98.93 ± 9.07 kJ/mol to 48.42 ± 2.28 kJ/mol. Previous studies have reported E_a values for oil-based PUFs under compression ranging from 25 to 80 kJ/mol, indicating that for the bio-based PUFs studied in this work, more energy is needed to influence their mechanical properties. The elevated RH condition facilitates the degradation process and might be one factor lowering E_a values; thus, in drier environments, the E_a could be even higher.[54–56] However, Slater et al.[56] reported an E_a of 25 kJ/mol for PUFs that were both dry and submerged in water. Therefore, castor oil PUFs are more likely to retain their initial mechanical properties than several oil-based ones, and their aging process should be slower than that of conventional PUFs.

4.3 | Acceleration prediction

Once the PUF aging properties have been acquired, it is possible to estimate the lifespan of the bio-based foam by

15482634, 0, Downloaded from https://4spepublications.onlinelibrary.wiley.com/doi/10.1002/pen.26725 by Univ of Sao Paulo - Brazil, Wiley Online Library on [19/04/2024]. See the Terms and Conditions (https://onlinelibrary.wiley.com/terms-and-conditions) on Wiley Online Library for rules of use; OA articles are governed by the applicable Creative Commons License

TABLE 5 Lifespan prediction for the bio-based PUF at operation conditions of 20, 30, and 40°C.

Temperature of operation (°C)	Direction	Lifespan prediction (years)	
		$E_r = 50\%$	$S_r = 50\%$
20	1	22.7	102
	3	9.8	9.5
30	1	6.3	26.7
	3	3.2	4.9
40	1	1.9	7.6
	3	1.1	2.7

considering a limit P_r value. For instance, Hong et al.[32] calculated the lifespan of a PU elastomer following the ASTM D2000-18,[33] which specifies that at a tensile strength retention of 70%, the material has reached its lifespan. Maxwell et al.[57] reported several ways to estimate the lifespan of materials due to different factors, and one of them is thermal aging and the half-life of its properties, where the P_r values achieve 50%. Thus, in the absence of specific standards for cellular materials or core materials for sandwich panels, the same P_r value will be considered in order to predict the lifespan of this foam. Additionally, room temperatures of 20, 30, and 40°C will be used as operational temperatures, as they are more common day-to-day values.

Equation 7 shows how to calculate the time necessary to achieve the ultimate retention (t_r) by the scheme shown in Figure 3:

$$\ln\frac{1}{(t_r)} = \ln\frac{1}{(t_1)} - \frac{E_a}{R}\left(\frac{1}{T_1} - \frac{1}{T_r}\right), \tag{7}$$

as three operational temperatures are used for lifespan estimation, Table 5 summarizes the predictions and shows that the predictions for Dir1 and Dir3 differ between each other. Since the Ea^{σ} was very different between both directions, Dir3 would need less energy to have its properties permanently changed, resulting in a shorter lifespan prediction.

Furthermore, it is worth pointing out that with the data presented in this paper, researchers and engineers will be able to estimate the lifespan of their specific vegetable-based PUF according to their specified P_r and temperature of operation.

5 | CONCLUSIONS

This study provides valuable insights into the aging process of vegetable-based PUFs. The foam synthesis was conducted meticulously in the laboratory, yielding specimens with standardized density. Through comprehensive testing of 100 specimens in two directions, we evaluated the aging effects longitudinally and transversely to the expansion. Analysis of cellular geometry was correlated with mechanical properties in each direction, highlighting the importance of understanding and controlling cell shape for tailored material properties in specific applications. Following aging at three different temperatures and 90% RH, the specimens underwent significant mass and volume changes, leading to increased density, particularly in those aged at 90°C. This rise in density influenced the plastic region of compression tests, resulting in early densification and postponement of maximum energy absorption efficiency to higher strains. This insight is crucial for designing castor oil-based foams targeted at energy absorption, as it clarifies the property changes after aging in elevated air humidity environments. The elasticity modulus decreased with harsher aging conditions, consistent with Arrhenius law predictions. However, an erratic behavior was observed for σc in Dir3 at 60°C, attributed to significant sample deviation typical of cellular materials and the relatively low aging temperature's minimal impact on material properties. Nonetheless, other conditions exhibited linear plots, as seen in Figures 11 and 12. The relatively high E_a values indicate good mechanical stability for this bio-based PUF, potentially surpassing some oil-based foams. Moreover, the calculated lifespan for P_r of 50% based on the activation energy of its compression properties provides crucial insights for applications of castor oil-based PUFs in sandwich structures. Understanding the mechanical property stability enhances the reliability of materials containing this foam, promoting a sustainable shift away from petroleum-based foams and reducing greenhouse gas emissions associated with oil refining. Overall, this study offers valuable information for implementing castor oil-based PUFs across various applications, furthering sustainability efforts in the materials industry.

ACKNOWLEDGMENTS

This research paper was founded by Coordenação de Aperfeicoamento de Pessoal de Nível Superior (CAPES)

15482634, 0, Downloaded from https://4spepublications.onlinelibrary.wiley.com/doi/10.1002/pen.26725 by Univ of Sao Paulo - Brazil, Wiley Online Library on [19/04/2024]. See the Terms and Conditions (https://onlinelibrary.wiley.com/terms-and-conditions) on Wiley Online Library for rules of use; OA articles are governed by the applicable Creative Commons License

process number 88887.716088/2022-00 and Conselho Nacional de Desenvolvimento Científico e Tecnológico (CNPq) process number 141012/2021-8.

DATA AVAILABILITY STATEMENT

The detailed data presented in this work can be provided under reasonable request.

ORCID

Enio Henrique Pires Da Silva https://orcid.org/0000-0003-1843-9735
Silvio De Barros https://orcid.org/0000-0002-2520-569X
Pascal Casari https://orcid.org/0000-0001-5939-7581
Marcelo Leite Ribeiro https://orcid.org/0000-0002-5586-2500

REFERENCES

1. Çakmakçı E, Özdemir M, Şen F, Bulut M, Yalçın B. Vegetable oil-based, coumarin-containing antibacterial thermosets with improved thermal stability via copper-free thermal azide-alkyne click polymerization. *Industr Crops Products*. 2022;182:114870. doi:10.1016/j.indcrop.2022.114870
2. Quilez-Molina AI, Mazzon G, Athanassiou A, Perotto G. A novel approach to fabricate edible and heat sealable bio-based films from vegetable biomass rich in pectin. *Mater Today Commun*. 2022;32:103871. doi:10.1016/j.mtcomm.2022.103871
3. Quilez-Molina AI, Merino D. Chapter 3 - from waste to resource: methods for vegetable waste transformation into sustainable plant-based bioplastics. In: Ahmed S, Annu, eds. *Advanced Applications of Biobased Materials*. Elsevier; 2023:61-110.
4. Ates M, Karadag S, Eker AA, Eker B. Polyurethane foam materials and their industrial applications. *Polym Int*. 2022;71:1157-1163. doi:10.1002/pi.6441
5. European Isocyanate Producers Association. *Polyurethanes: Sustainable Applications*. ISOPA; 2001.
6. de Moura AP, da Silva EHP, dos Santos VS, et al. Structural and mechanical characterization of polyurethane-$CaCO_3$ composites synthesized at high calcium carbonate loading: an experimental and theoretical study. *J Compos Mater*. 2021;55:2857-2866. doi:10.1177/0021998321996414
7. Burelo M, Gaytán I, Loza-Tavera H, et al. Synthesis, characterization and biodegradation studies of polyurethanes: effect of unsaturation on biodegradability. *Chemosphere*. 2022;307:136136. doi:10.1016/j.chemosphere.2022.136136
8. Silva EHP, Souza GSC, Janes DB, et al. Flexural and flammability evaluation of a new bio-based polyurethane foam with alumina trihydrate. *Proc Inst Mech Eng J Mater Des Appl*. 2021;235:1160-1171. doi:10.1177/1464420720986591
9. Stirna U, Lazdiņa B, Vilsone D, et al. Structure and properties of the polyurethane and polyurethane foam synthesized from castor oil polyols. *J Cell Plast*. 2012;48:476-488. doi:10.1177/0021955X12445178
10. Lee JH, Kim SH, Oh KW. Bio-based polyurethane foams with Castor oil based multifunctional polyols for improved compressive properties. *Polymers*. 2021;13:576. doi:10.3390/polym13040576
11. Maiuolo L, Olivito F, Algieri V, et al. Synthesis, characterization and mechanical properties of novel bio-based polyurethane foams using cellulose-derived polyol for chain extension and cellulose citrate as a thickener additive. *Polymers*. 2021;13:2802. doi:10.3390/polym13162802
12. Silva EHP, Aguiar JCF, Waldow G, Costa RRC, Tita V, Ribeiro ML. Compression and morphological properties of a bio-based polyurethane foam with aluminum hydroxide. *Proc Inst Mech Eng Part L: J Mater Des Appl*. 2022;236:1408-1418. doi:10.1177/14644207211059077
13. Wang J, Zhang C, Deng Y, Zhang P. A review of research on the effect of temperature on the properties of polyurethane foams. *Polymers*. 2022;14:4586. doi:10.3390/polym14214586
14. Kaikade DS, Sabnis AS. Recent advances in polyurethane coatings and adhesives derived from vegetable oil-based polyols. *J Polym Environ*. 2023;31:4583-4605. doi:10.1007/s10924-023-02920-z
15. Gibson LJ, Ashby MF. *Cellular Solids: Structure & Properties*. Cambridge Cambridge University Press; 1997.
16. Lakes R. Foam structures with a negative Poisson's ratio. *Science*. 1987;235:1038-1040. doi:10.1126/science.235.4792.1038
17. Boubakri A, Guermazi N, Elleuch K, Ayedi HF. Study of UV-aging of thermoplastic polyurethane material. *Mater Sci Eng A*. 2010;527:1649-1654. doi:10.1016/j.msea.2010.01.014
18. Pritchard G. *Plastics Additives: An A-Z Reference*. Springer, S. L; 1998.
19. Chattopadhyay DK, Webster DC. Thermal stability and flame retardancy of polyurethanes. *Prog Polym Sci*. 2009;34:1068-1133. doi:10.1016/j.progpolymsci.2009.06.002
20. Bilbao R, Mastral JF, Ceamanos J, Aldea ME. Kinetics of the thermal decomposition of polyurethane foams in nitrogen and air atmospheres. *J Anal Appl Pyrolysis*. 1996;37:69-82. doi:10.1016/0165-2370(96)00936-9
21. Yarahmadi N, Vega A, Jakubowicz I. Accelerated ageing and degradation characteristics of rigid polyurethane foam. *Polym Degrad Stab*. 2017;138:192-200. doi:10.1016/j.polymdegradstab.2017.03.012
22. Gupta T, Adhikari B. Thermal degradation and stability of HTPB-based polyurethane and polyurethaneureas. *Thermochimica Acta*. 2003;402:169-181. doi:10.1016/S0040-6031(02)00571-3
23. Hablot E, Zheng D, Bouquey M, Averous L. Polyurethanes based on castor oil: kinetics, chemical, mechanical and thermal properties. *Macromol Mater Eng*. 2008;293(11):922-929. doi:10.1002/mame.200800185
24. Berardi U. The impact of aging and environmental conditions on the effective thermal conductivity of several foam materials. *Energy*. 2019;182:777-794. doi:10.1016/j.energy.2019.06.022
25. Taguti MVH, Françoso A, Ribeiro ML, Vieira AFC. Numerical approach to simulate the mechanical behavior of biodegradable structures considering degradation time and heterogeneous stress field. *Polym Eng Sci*. 2020;60:1566-1578. doi:10.1002/pen.25402
26. Vieira AFC, da Silva EHP, Ribeiro ML. Numerical approach to simulate the mechanical behavior of biodegradable polymers during erosion. *Polymers*. 2023;15:1979. doi:10.3390/polym15091979
27. Deng M, Zhou J, Chen G, et al. Effect of load and temperature on in vitro degradation of poly(glycolide-co-l-lactide) multifilament braids. *Biomaterials*. 2005;26:4327-4336. doi:10.1016/j.biomaterials.2004.09.067
28. Guo M, Chu Z, Yao J, et al. The effects of tensile stress on degradation of biodegradable PLGA membranes: a quantitative

15482634, 0, Downloaded from https://4spepublications.onlinelibrary.wiley.com/doi/10.1002/pen.26725 by Univ of Sao Paulo - Brazil, Wiley Online Library on [19/04/2024]. See the Terms and Conditions (https://onlinelibrary.wiley.com/terms-and-conditions) on Wiley Online Library for rules of use; OA articles are governed by the applicable Creative Commons License

study. *Polym Degrad Stab*. 2016;124:95-100. doi:10.1016/j.polymdegradstab.2015.12.019

29. Li DH. Extended layerwise method of laminated composite shells. *Compos Struct*. 2016;136:313-344. doi:10.1016/j.compstruct.2015.08.141
30. Tsuji H, Nakahara K. Poly(L-lactide). IX. Hydrolysis in acid media. *J Appl Polym Sci*. 2002;86:186-194. doi:10.1002/app.10813
31. Liu Y, Wang H, du J, Lin J, Cao Y, Cheng L. Comparative experimental study on mechanical properties of CFRP subjected to seawater and hydrostatic pressure. *Compos Sci Technol*. 2023;242:110193. doi:10.1016/j.compscitech.2023.110193
32. Hong S, Park NY, Ju S, et al. Molecular degradation mechanism of segmented polyurethane and life prediction through accelerated aging test. *Polym Test*. 2023;124:108086. doi:10.1016/j.polymertesting.2023.108086
33. American Society for Testing and Materials (ASTM). *ASTM D2000-18 - Standard Classification System for Rubber Products in Automotive Applications*. ASTM International; 2018.
34. Tita V, Caliri MF Júnior, Angélico RA, Canto RB. Experimental analyses of the poly(vinyl chloride) foams' mechanical anisotropic behavior. *Polym Eng Sci*. 2012;52:2654-2663. doi:10.1002/pen.23222
35. Tagarielli VL, Deshpande VS, Fleck NA, Chen C. A constitutive model for transversely isotropic foams, and its application to the indentation of balsa wood. *Int J Mech Sci*. 2005;47:666-686. doi:10.1016/j.ijmecsci.2004.11.010
36. Taourit S, le Gac PY, Fayolle B. Relationship between network structure and ultimate properties in polyurethane during a chain scission process. *Polym Degrad Stab*. 2022;201:109971. doi:10.1016/j.polymdegradstab.2022.109971
37. Liu R, Li S, Yao N, et al. Castor oil-based polyurethane networks containing diselenide bonds: self-healing, shape memory, and high flexibility. *Prog Org Coat*. 2022;163:106615. doi:10.1016/j.porgcoat.2021.106615
38. Langueh C, Changotade S, Ramtani S, Lutomski D, Rohman G. Combination of in vitro thermally-accelerated ageing and Fourier-transform infrared spectroscopy to predict scaffold lifetime. *Polym Degrad Stab*. 2021;183:109454. doi:10.1016/j.polymdegradstab.2020.109454
39. Arczewska P, Polak MA, Penlidis A. Degradation of glass fiber reinforced polymer (GFRP) bars in concrete environment. *Construct Build Mater*. 2021;293:123451. doi:10.1016/j.conbuildmat.2021.123451
40. Tham WL, Poh BT, Mohd Ishak ZA, Chow WS. Water absorption kinetics and Hygrothermal aging of poly(lactic acid) containing Halloysite Nanoclay and Maleated rubber. *J Polym Environ*. 2015;23:242-250. doi:10.1007/s10924-014-0699-y
41. Nelson W. *Accelerated Testing*. John Wiley & Sons, Inc; 1990.
42. Panaitescu I, Koch T, Archodoulaki VM. Accelerated aging of a glass fiber/polyurethane composite for automotive applications. *Polym Test*. 2019;74:245-256. doi:10.1016/j.polymertesting.2019.01.008
43. Da Silva EHP, De Barros S, Vieira AFC, Da Costa RRC, Ribeiro ML. Accelerated aging on the compression properties of a green polyurethane foam: experimental and numerical analysis. *Polymers*. 2023;15:1784. doi:10.3390/polym15071784
44. ASTM. *D1621 – Standard Test Method for Compressive Properties of Rigid Cellular Plastics*. ASTM – American Standard Test Method; 2016.
45. Andersons J, Kirpluks M, Cabulis P, Kalnins K, Cabulis U. Bio-based rigid high-density polyurethane foams as a structural thermal break material. *Construct Build Mater*. 2020;260:120471. doi:10.1016/j.conbuildmat.2020.120471
46. Rahimidehgolan F, Magliaro J, Altenhof W. Influence of specimen profile size and thickness on the dynamic compressive behavior of rigid PVC foams. *Int J Impact Eng*. 2023;179:104676. doi:10.1016/j.ijimpeng.2023.104676
47. Silva NGS, Cortat LICO, Teixeira EJO, Baptista L, Orlando D, Mulinari DR. Influence of natural exposure on castor oil based polyurethane reinforced with waste tire rubber. *Waste Manag*. 2023;155:220-229. doi:10.1016/j.wasman.2022.11.004
48. Li P, Guo YB, Shim VPW. A constitutive model for transversely isotropic material with anisotropic hardening. *Int J Solids Struct*. 2018;138:40-49. doi:10.1016/j.ijsolstr.2017.12.026
49. Yao B, Ye R, Li Z, Liu M, Liu Y. Compressive properties and energy absorption of honeycomb filled square tubes produced by selective laser melting. *Mater Sci Eng A*. 2022;847:143259. doi:10.1016/j.msea.2022.143259
50. Kim J-D, Kim JH, Lee DH, Yeom DJ, Lee JM. Synthesis and investigation of cryogenic mechanical properties of chopped-glass-fiber-reinforced Polyisocyanurate foam. *Materials*. 2021;14:446. doi:10.3390/ma14020446
51. Jabli M, Sebeia N, Bchetnia A. Synthesis and characterization of pectin-manganese oxide and pectin-tin oxide nanocomposites: application to the degradation of Calmagite in water. *J Polym Environ*. 2023;31:4326-4337. doi:10.1007/s10924-023-02888-w
52. Al-Moameri H, Ghoreishi R, Zhao Y, Suppes GJ. Impact of the maximum foam reaction temperature on reducing foam shrinkage. *RSC Adv*. 2015;5:17171-17178. doi:10.1039/C4RA12540A
53. Kissinger HE. Reaction kinetics in differential thermal analysis. *Anal Chem*. 1957;29:1702-1706. doi:10.1021/ac60131a045
54. Assink RA, Celina MC, Eliott JM. *Thermal Aging of the Polyurethane Foamfor the H1259 Storage Container*. Sandia National Laboratories; 2006.
55. Lee S-W, Park J-Y, Park E-Y, et al. Evaluation of static spring constant and accelerated life prediction for compression set of polyurethane resilient pad in rail fastening system. *Elastomers Compos*. 2018;53(4):220-225.
56. Slater C, Davis C, Strangwood M. Compression set of thermoplastic polyurethane under different thermal–mechanical-moisture conditions. *Polym Degrad Stab*. 2011;96:2139-2144. doi:10.1016/j.polymdegradstab.2011.09.012
57. Maxwell AS, Broughton WR, Dean G, Sims G. Review of accelerated ageing methods and lifetime prediction techniques for polymeric materials. 2005.

How to cite this article: Da Silva EHP, De Barros S, Casari P, Ribeiro ML. Aging properties of a vegetable-based polyurethane foam under high relative humidity and different temperatures. *Polym Eng Sci*. 2024;1-17. doi:10.1002/pen.26725

15482634, 0, Downloaded from https://4spepublications.onlinelibrary.wiley.com/doi/10.1002/pen.26725 by Univ of Sao Paulo - Brazil, Wiley Online Library on [19/04/2024]. See the Terms and Conditions (https://onlinelibrary.wiley.com/terms-and-conditions) on Wiley Online Library for rules of use; OA articles are governed by the applicable Creative Commons License